Luca Fambri

POLY(LACTIC ACID)

Synthesis, Structures, Properties, Processing, and Applications

Edited by

RAFAEL AURAS
LOONG-TAK LIM
SUSAN E. M. SELKE
HIDETO TSUJI

WILEY
A JOHN WILEY & SONS, INC., PUBLICATION

9

CRYSTALLIZATION AND THERMAL PROPERTIES

LUCA FAMBRI AND CLAUDIO MIGLIARESI

9.1 INTRODUCTION

Poly(lactic acid) (PLA)-based products have been largely considered for both biomedical and environment-friendly applications [1–9]. Processing conditions and final properties of PLAs are strongly determined/influenced by the crystalline or amorphous structure of the polymer [10–12].

Starting from the early work of Kulkarni et al. [13, 14] in 1966 and 1971, many papers addressed the evaluation of thermal properties and crystallinity of PLA or polylactide-based polymers.

The chiral nature of lactic acid results in distinct forms of polylactide, namely, poly(L-lactide) (PLLA), poly(D-lactide) (PDLA), and poly(DL-lactide) (PDLLA), which are synthesized from the L-, D-, and DL-lactic acid monomers, respectively, or from the corresponding L,L-lactide, D,D-lactide, and DL-lactide, respectively [15].

Both L- and D-lactic acid stereoisomers are naturally occurring; however, most of the lactic acid in nature is L-type or sometimes racemic. The fact that lactic acid that is produced in the human body is in the L-enantiomeric form and the interest in the biomedical applications of this polymer have led both research and production to concentrate on L-lactide or DL-lactide polymers [16–18]. The D-isomer does not have many applications, except for use in particular medicinal chemicals.

Today petrochemical-based production gives a 50/50 mixture of the L- and D-forms, whereas from fermentation mostly L-lactic acid is obtained. Recently, new research has been reported on the production of D-lactic acid from rice fermentation [19].

PLLA and PDLA are crystalline polymers due to the enantiomeric purity of the pristine monomers and the stereoregularity of the polymer chain. Conversely, PDLLA, which is an equimolar relatively random copolymer of L- and D-lactic acid (or L- and D-lactide), is fully amorphous because of its irregular structure. The stereochemical configuration of PLLA (or PDLA) and PDLLA is analogous to that of isotactic polypropylene and atactic polypropylene. Syndiotactic PLA that can be polymerized from a stereoselective polymerization of *meso*-lactide can be considered as an alternating DL-lactic acid copolymer, analogous to syndiotactic polypropylene [20].

Worth noting is the fact that in the early work of Kulkarni et al. [14] the glass transition peak of PDLLA at about 60°C was misinterpreted and attributed to melting. Pure PLLA and PDLA have the same properties, that is, a glass transition temperature (T_g) between 50 and 70°C, a melting temperature (T_m) between 170 and 190°C, and a crystallinity of around 35% [1, 2, 7, 8, 21–28]. In the case of syndiotactic polylactide, due to the different stereotactic configuration, lower glass transition temperature and melting temperature were found to be 34 and 155°C, respectively [20]. Crystallization, crystallinity degree, and thermal properties of PLLA depend on the polymer molecular weight, polymerization conditions, thermal history, purity, and so on. As reported by Ikada et al. [25], blending of PLLA and PDLA results in the formation of a stereocomplex with a crystalline structure different from that of each homopolymer and melting temperatures that reach 230°C [25]. Contradictory data are reported about PLLA melting enthalpy, ranging in the literature from 40 to 203 J/g. The most common values adopted for the melting enthalpy of PLLA are 93.6 J/g, as reported by Fisher et al. [21], or 140 J/g, as evaluated by Loomis et al. [29].

Many authors have studied the crystalline structure of PLLA [30–45]. PLLA crystals present three different

Poly(lactic acid): Synthesis, Structures, Properties, Processing, and Applications, edited by R. Auras, L.-T. Lim, S. E. M. Selke, and H. Tsuji
Copyright © 2010 John Wiley & Sons, Inc.

structural conformations that can develop under different processing or treatment conditions [42]. In particular, melt or cold crystallization and solution spinning processes at low drawing temperatures and/or low hot draw ratios induce the formation of α-structures characterized by a left-handed 10_3 helix that packs in an orthorhombic unit cell with parameters $a = 1.06$ nm, $b = 1.737$ nm, and $c = 2.88$ nm [46]. Stretching, solution spinning, or high hot draw ratios induce the formation of β-crystal structures, a unit cell with $a = 1.031$ nm, $b = 1.821$ nm, and $c = 0.900$ nm, and a chain conformation with left-handed 3_1 helices [47]. More recently, an additional crystalline form named γ that develops under epitaxial crystallization has been reported [48].

9.2 CRYSTALLINITY AND CRYSTALLIZATION

Figure 9.1 shows a typical differential scanning calorimetry (DSC) analysis of thermal behavior of two amorphous PLAs, that is, a PDLLA ($M_w = 70$ kDa) sample that is intrinsically amorphous and PLLA ($M_w = 200$ kDa) that was quenched to the amorphous state by fast cooling at −100°C/min after melting. In both cases, the T_g is evident and is located at about 65°C.

Above T_g, PDLLA exhibits an aging peak in the interval 65–90°C with an enthalpy of 8 J/g, typical of amorphous polymer aging. The longer the aging time and/or the closer the aging temperature to the T_g, the more intense is that peak. PDLLA can reach an enthalpy value of about 10 J/g, as shown by Celli and Scandola [28]. On the other hand, the initial amorphous PLLA presents a broad crystallization peak in the range 100–160°C centered at about 132°C with $\Delta H_c = 38$ J/g, followed by melting at 182°C with $\Delta H_m = 38$ J/g. As determined by the equal values of the crystallization and melting enthalpies, the fast quenching produced a fully amorphous material. The variation of specific heat (ΔC_p) at T_g was 0.50 J/(g K).

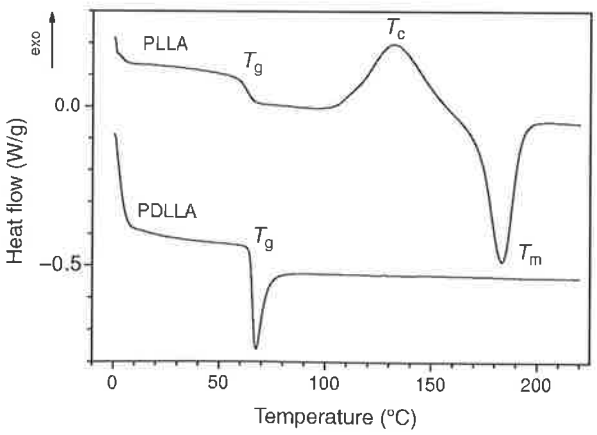


FIGURE 9.1 Differential scanning calorimetry thermograms of amorphous PLLA and PDLLA (heating rate 10°C/min).

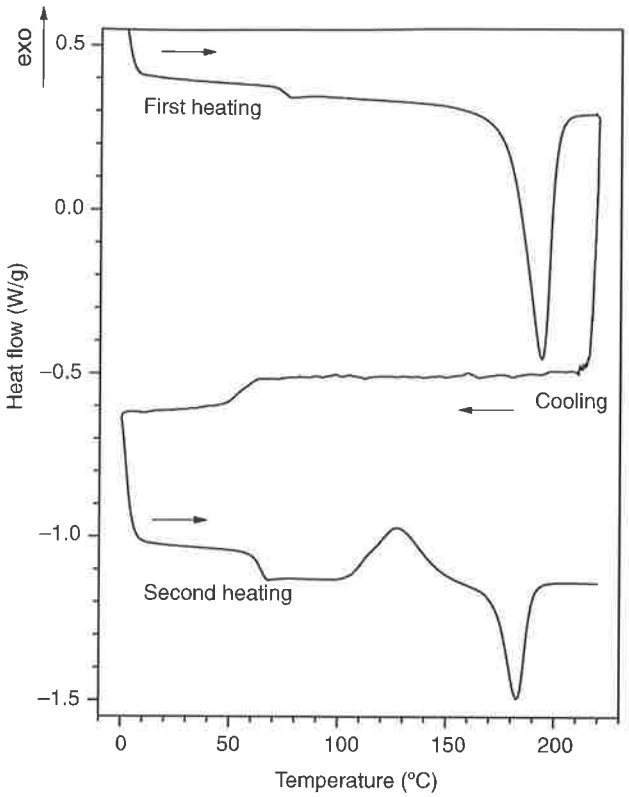


FIGURE 9.2 DSC thermal cycles of PLLA 200 kDa (first heating, cooling, and second heating at ±10°C/min).

Figure 9.2 refers to a commercial PLLA (L210 from Boehringer, Ingelheim, Germany) with a molecular weight of 200 kDa, subjected to the following three DSC runs at 10°C/min: (i) heating from 0 to 220°C, (ii) cooling from 220 to 0°C, and finally (iii) heating from 0 to 220°C. The initially crystalline polymer presented a T_g at 73°C and melted at 192°C. During cooling, apparently no crystallization developed and the following thermal run on the initially amorphous materials showed glass transition (at $T_g = 64$°C), crystallization (at $T_c = 127$°C), and melting (at $T_m = 181$°C). Worth noting between the curves of Figures 9.1 and 9.2 is the difference in the crystallization temperature, which was lower for the slowly cooled polymer, probably due to the formation of crystallization nuclei during cooling.

Table 9.1 lists T_g, T_m, T_c, ΔH_c, and ΔH_m of various molecular weight PLLA samples, namely, 2, 30, and 200 kDa, respectively, subjected to the same DSC cycles presented in Figure 9.2.

The crystallinity content (X) has been evaluated from the DSC data according to the following equation:

$$X\% = 100(\Delta H_m - \Delta H_c)/\Delta H_m^0 \qquad (9.1)$$

where ΔH_m and ΔH_c are the melting and the crystallization enthalpies, respectively, and ΔH_m^0 is the reference ΔH_m (93.6 J/g) for PLLA crystals having an infinite size [21].

TABLE 9.1 Glass Transition Temperature (T_g) and Change of Specific Heat at T_g (ΔC_p), Melting Peak Temperature (T_m) and Enthalpy (ΔH_m), and Crystallization Peak Temperature (T_c) and Enthalpy (ΔH_c) for Different Molecular Weight of PLLA Samples During a DSC Cycle of Heating–Cooling–Heating Between 0 and 220°C at ±10°C/min

(i) First Heating

M_W (kDa)	T_g (°C)	ΔC_p (J/(g K))	T_m (°C)	ΔH_m (J/g)	X (%)
2	58	0.17	147	48	51
30	79	0.06	171	68	73
200	73	0.22	192	67	72

(ii) Cooling

M_W (kDa)	T_c (°C)	ΔH_c (J/g)	T_g (°C)	ΔC_p (J/(g K))
2	–	–	39	0.56
30	96	21	50	0.32
200	–	–	55	0.50

(iii) Second Heating

M_W (kDa)	T_g (°C)	ΔC_p (J/(g K))	T_c (°C)	ΔH_c (J/g)	T_m (°C)	ΔH_m (J/g)	X (%)
2	43	0.54	107	9	142	9	0
30	55	0.32	97	21	174	50	31
200	64	0.51	127	25	181	26	1

Due to the favorable crystallization conditions during the polymerization process, all the products in the first scan display a high crystallinity between 50% and 73%, depending on their molecular weight, and melting temperature that is proportional to the molecular weight according to the classical Flory equation

$$1/T_m = 1/T_m^* - 2RM_0/\Delta H_{mu}M_n \qquad (9.2)$$

where T_m is the melting temperature, T_m^* is the melting temperature at infinite molecular weight, R is the gas constant, ΔH_{mu} is the heat of fusion per mole of the repeating unit, M_0 the molecular weight of the repeating unit, and M_n is the number-average molecular weight.

The Flory–Fox equation

$$T_g = T_g^* - K/M_n \qquad (9.3)$$

can also be used to predict the T_g of polymers as a function of the molecular weight, T_g^* being the T_g at infinite M_n.

While the first heating T_g values are higher than expected due to high crystallinity content (crystalline domains hinder the mobility of amorphous chains), as also confirmed from the low value of ΔC_p at T_g, T_g measured during cooling proportionally depend on molecular weight, in accordance with Equation 9.3.

It is also interesting to note that during cooling PLLA (30 kDa) developed some crystallinity, whereas in the other cases crystallization was inhibited by the high content of terminal groups that acted as defects in PLLA (2 kDa) and by the low mobility of the long PLLA (200 kDa) chains.

During the second heating, all the polymers evidenced glass transition, crystallization, and melting. T_g and T_m directly depend on molecular weight. The different T_g values measured during cooling and the following heating cycles of the amorphous PLLAs, that is, 39 versus 43°C for the 2 kDa PLLA and 55 versus 64°C for the 200 kDa PLLA, are due to a kinetic effect that depends on the molecular weight of the polymer. The lower T_c of PLLA (30 kDa) is attributable to its crystallinity before the second heating cycle that acted as a nucleating agent and promoted further crystallization, up to 53%, as determined from the melting enthalpy. In the case of PLLA (2 kDa) and PLLA (200 kDa), the lower ΔH_m and crystallinity of about 10% and 28%, respectively, once again directly depend on the effect of short and long polymer chains.

As a function of molecular weight, however, the same or different thermal treatments can produce different results, as clearly shown by Migliaresi et al. [27, 32] and summarized in Figure 9.3. The crystallinity of the polymers shown in Figure 9.3 increases with annealing time and with decreasing viscometric molecular weight (M_v). Almost slowly and progressively increasing constant values were reached faster by the lower molecular weight PLLAs. This increase, as discussed later in the chapter, could be attributed not only to kinetic effects but also to thermal degradation of M_v during annealing. This effect has not often been considered in the literature.

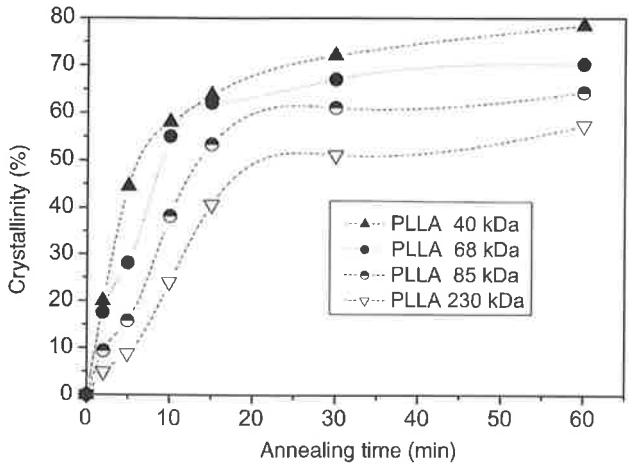


FIGURE 9.3 Effect of annealing time on crystallinity of compression molded PLLA at 160°C (adapted from Ref. 32).

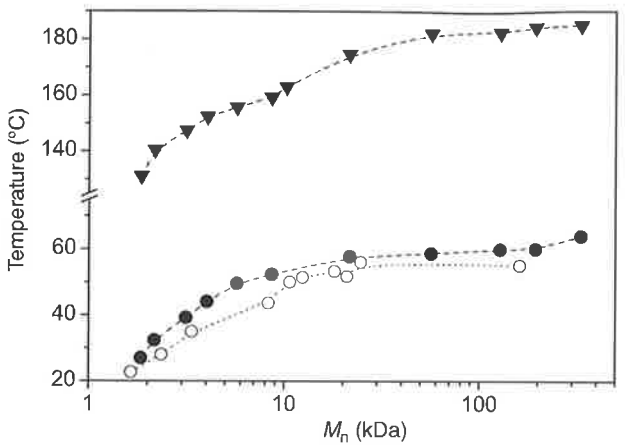


FIGURE 9.4 Melting temperature of PLLA (▼) and glass transition temperature of PLLA (●) and PDLLA (○) polymer as a function of molecular weight (adapted from Ref. 31 and authors' data).

Migliaresi et al. [27] showed that low molecular weight PLLA ($M_v = 18$ kDa) was able to crystallize regaining almost 65%, 79%, and 87% of its initial crystallinity, during cooling after full melting at −5, −1, and −0.5°C/min, attaining crystallinity contents of 38.5%, 46.8%, and 51.3%, respectively. Higher M_v PLLA (156 and 425 kDa) developed only a little crystallinity when cooled at −5°C/min. As pointed, mobility, and hence crystallization ability, is determined, at any given molecular weight, by the temperature of the system. Their data confirmed that same thermal histories lead to materials with substantially different crystallinity amounts as a function of the PLLA molecular weight. More important perhaps, Migliaresi et al. [27] evidenced that any treatment always caused molecular weight degradation, as shown in Table 9.2. This also means that, at a given initial molecular weight, thermal cycles at different heating or cooling rates are representative of polymers having actually different viscometric molecular weight M_v.

The effect of molar mass on PLLA T_g and T_m and on PDLLA T_g is clearly shown in Figure 9.4. T_g values of both PLLA and PDLLA show similar trend with molar mass, with a glass transition increase up to about 20 kDa molar mass and an almost threshold value thereinafter. At each M_n, PLLA displays higher T_g, this being attributable to the hindering effect exerted on the amorphous chain mobility by the crystalline regions. Worth noting is the similar trend for melting, with T_m ranging from about 130 to about 180°C as a function of M_n.

The effect of the L- or D-content on the T_g of PLA has been discussed by Lim et al. [12] and Dorgan et al. [49]. The T_m of PLA is also a function of its optical purity. While the calculated theoretical T_m values for pure PLLA are reported to be 215, 207, and 205°C by different authors, the maximum practical obtainable T_m for pure PLLA is around 190°C [23, 35, 50].

The T_g is better evidenced in dynamical mechanical thermal analysis (DMTA) as shown in Figures 9.5 and 9.6, where the storage modulus E', loss modulus E'', and the damping or loss factor $\tan\delta = E''/E'$ are presented [51, 52]. In

TABLE 9.2 Effect of Cooling Rate C on the Residual Molar Mass of Different Viscometric Molecular Weight PLLAs, Previously Heated at 10°C/min to 220°C

Initial M_v (kDa)	After Cooling at C −100°C/min	After Cooling at C −20°C/min	After Cooling at C −5°C/min
18	15 (−17%)	14 (−22%)	11 (−39%)
31	26 (−16%)	26 (−16%)	25 (−19%)
156	113 (−28%)	111 (−29%)	75 (−52%)
425	364 (−15%)	357 (−16%)	225 (−49%)

Note: Reprinted from Ref. 27. Copyright 1991, with permission from Elsevier.

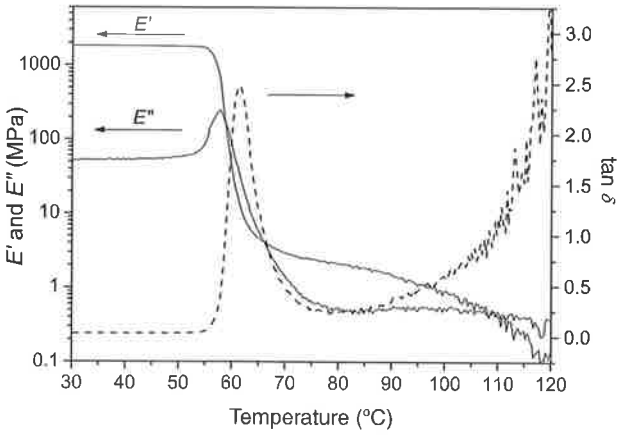


FIGURE 9.5 Storage modulus E', loss modulus E'', and damping $\tan\delta$ of PDLLA. Heating rate 2°C/min and frequency 1 Hz.

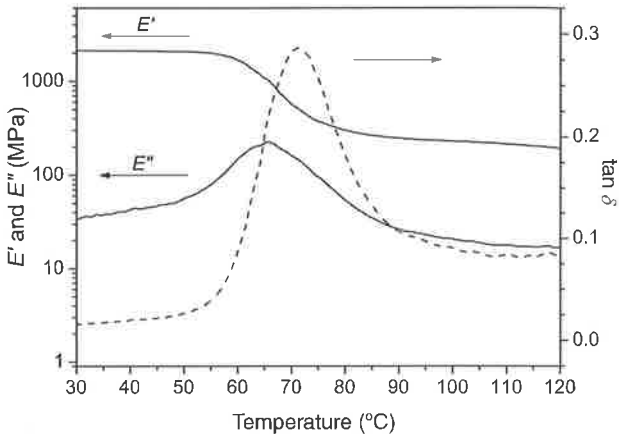


FIGURE 9.6 Storage modulus E', loss modulus E'', and damping tan δ of PLLA with a crystallinity of 55%. Heating rate 2°C/min and frequency 1 Hz.

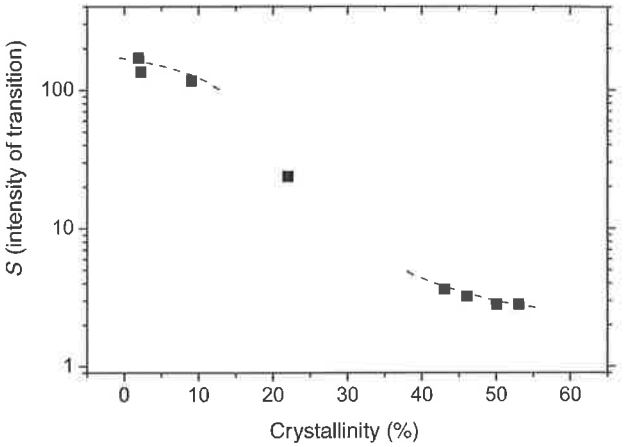


FIGURE 9.7 Effect of crystallinity on the intensity of the transition S of compression molded samples (data from Ref. 32).

these plots, the temperatures corresponding to the tan δ or E'' peaks are taken as the T_g values.

Both PDLLA (Figure 9.5) and PLLA (Figure 9.6) polymers exhibit a storage modulus in the glassy region of about 2 GPa with a slight difference due to the crystalline content of PLLA ($X = 55\%$). Crystallinity is, however, responsible for the much lower decrease of E' and E'' of PLLA after T_g and for the progressive increase of damping of PDLLA in the temperature range 100–120°C. Again, crystallinity accounts for the higher temperatures and width of the E'' peak of PLLA, both of them being due to the constraints exerted by the PLLA crystalline domains on the amorphous region mobility. Crystallinity, however, can have an important effect on PLLA mechanical properties and can be affected by the molecular weight. As shown by Perego et al. [39], crystallinity of PLLA of different viscometric molecular weights and annealed at 105°C for 90 min increased from 3–13% to 42–65%, depending on the molecular weight. While for low crystalline polymers, properties such as tensile strength or impact resistance almost did not depend on M_v, crystallization induced significant differences, improving these properties markedly for higher M_v polymers.

Following the approach of Diez-Gutierrez et al. [53] that studied the effect of filler on the mechanical properties of talc/polypropylene composites, Fambri et al. [54] analyzed the effect of crystallinity on the storage modulus E' of PLLA through a glass transition intensity factor defined as

$$S = (E'_g - E'_r)/E'_r \tag{9.4}$$

In Equation 9.4, E'_g and E'_r are the E' values in the glassy and rubbery states taken at about 30°C below and above the T_g, that is, 30 and 90°C, respectively.

Values of $S_{PDLLA} = 1173$ and $S_{PLLA} = 7.5$ were calculated from data of Figures 9.5 and 9.6. A higher S value indicates a superior mobility and/or a higher content of the amorphous phase. With increasing crystallinity, the intensity factor S decreases, with an almost proportional dependence on crystallinity (see Figure 9.7) for compression molded materials (data from Ref. 32).

Since the glass transition is a kinetic transition, the measured value depends on both heating rate and frequency. This is clearly evidenced by comparing DMTA curves of Figure 9.6 (at 2°C/min and 1 Hz) and the multifrequency DMTA analysis of Figure 9.8 (at 0.5°C/min and 3, 10, and 30 Hz). At increasing deformation frequencies, the storage moduli of the glassy and rubbery plateaus increase and the apparent T_g is shifted to higher temperatures.

The apparent activation energy for the relaxation process can be calculated from the following equation:

$$\ln f = \ln f_0 - (E_a/RT) \tag{9.5}$$

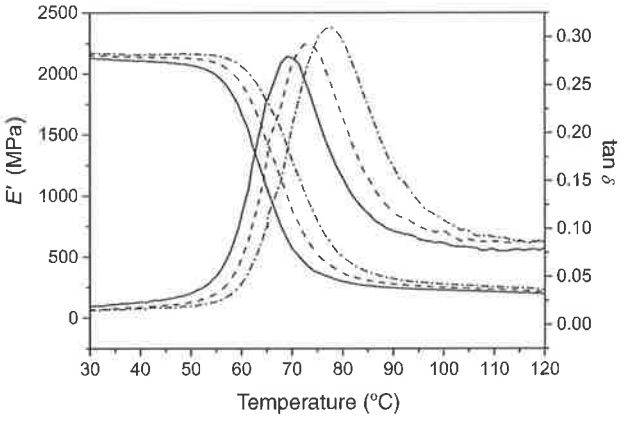


FIGURE 9.8 Storage modulus E' and damping factor tan δ of PLLA samples at various frequencies: 3 Hz (continuous line), 10 Hz (dashed line), and 30 Hz (dash-dotted line). Heating rate 0.5°C/min (from authors' data).

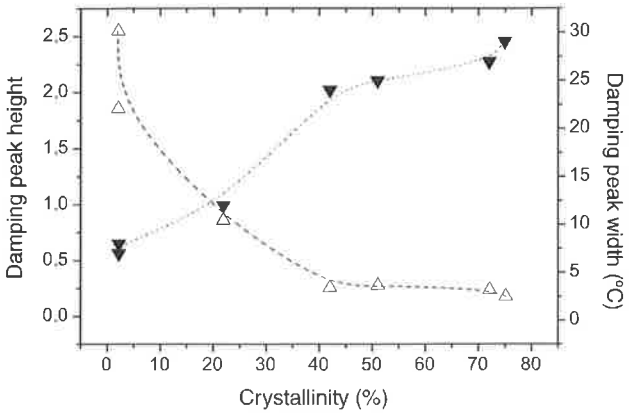


FIGURE 9.9 Height (△) and width (▼) of damping peak of PLLA as a function of crystallinity (data from Ref. 32).

where f is the frequency in Hz, T is the temperature of the maximum of the loss factor, R is the ideal gas constant, and E_a is the activation energy for the relaxation process. According to Equation 9.5, apparent E_a of 553 and 620 kJ/mol were calculated for low and high molecular weight PLLA, respectively [53].

In dynamic mechanical tests, the reduced chain mobility due to the crystalline domains is detected by the shift of the damping peak to higher temperatures, that is, the increase of T_g, as already stated for DSC analyses. In addition, as shown in Figure 9.9, the DMTA evidences an increase of the elastic component of the viscoelastic behavior of the polymer as a significant reduction of the damping peak (data from Ref. 32).

At the same time, the width of the tan δ peak increases as an effect of the larger distribution of amorphous chain mobility induced by the formation of a less mobile distributed interphase [55, 56].

In practical injection molding conditions, there is little crystallization due to the high cooling rate. For this reason, methods to induce crystallization have been studied by using nucleating agents or plasticizers during polymer processing. By using 1% talc, the crystallization half time can be reduced to less than 1 min [57]. Other nucleating agents such as montmorillonite are less effective than talc [58]. Some organic compounds have also been studied, such as calcium lactate, *N,N*-ethylenebis(12-hydroxystearamide), benzoylhydrazide compounds, or sodium stearate [59–62]. Addition of 1% calcium lactate induced crystallization of a 90:10 L/D, L-PLA copolymer during the injection molding cycle [59].

Kawamoto et al. [61] found that in the presence of a series of hydrazide compounds having a variety of methylene chain numbers, the T_c, and ΔH_c, of PLLA during cooling increased with the methylene chain number. In this study, decamethylene dicarboxylic dibenzoylhydrazide was the most effective in promoting crystal nucleation by increasing the PLA T_c and ΔH_c to 131°C and 46 J/g, respectively. The addition of a plasticizer decreases the T_g. Common plasticizers used for PLA are poly(ethylene glycol), triacetine, and citrate, laurate, and sebacate esters [26, 62–68]. The primary effect is the improvement of the polymer ductility and drawability, but also an increase of crystallization rate, as shown by Kulinski and Piorkowska [66] for PEG added PLLA.

9.3 CRYSTALLIZATION REGIME

One of the first papers discussing the morphology and crystal growth of PLLA as a function of thermal treatment and molecular weight was published by Vasanthakumari and Pennings in 1983 [30]. Following Hoffman and coworkers [69, 70], the growth rate (G) of a linear polymer crystal with chain folding can be expressed by

$$G = G_0 \exp\left[\frac{-u^*}{R(T_c - T_\infty)}\right] \exp\left[\frac{-K_g}{T_c \Delta T f}\right] \qquad (9.6)$$

where K_g is the nucleation constant, u^* is the activation energy of chain mobility in the crystallization site, $\Delta T = (T_m^0 - T_c)$ is the difference between the equilibrium melting temperature and the crystallization temperature, f is a factor equal to $2T_c/(T_m + T_c)$, R is the gas constant, T_∞ is the temperature at which all the motion associated with viscous flow ceases, and G_0 is the front factor. Equation 9.6 can be used to predict the crystallization rate of a number of polymers over a wide range of temperature.

As reported in Figure 9.10, the spherulite radius growth rate as a function of T_c reached a maximum for all investigated molecular weights at temperatures ranging around 130°C and depending on the specific polymer molecular weight [30].

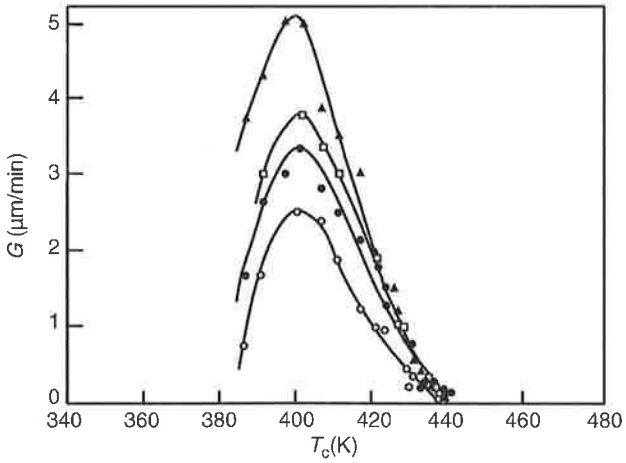


FIGURE 9.10 Radius growth rate G as function of crystallization temperature T_c for different viscometric molecular weight samples of PLLA, that is, $M_v = 150$ kDa (▲), 260 kDa (□), 350 kDa (●), and 690 kDa (○). Reprinted from Ref. 30. Copyright 1983, with permission from Elsevier.

In particular, the higher the PLLA molecular weight, the lower the G, as generally observed for many polymers. Different cooling rates also induced variation in the crystal morphology, with the formation of regular geometry and defined spherulites at high undercooling and spherulites with irregular shape and a coarse-grained structure at lower ΔT.

According to the Hoffman theory, polymers such as polyethylene present two different crystallization regimes characterized by the ratio of the corresponding nucleation constants K_{gI}/K_{gII} equal to 2 [69, 70]. The presence of two crystallization regimes was confirmed by Vasanthakumari and Pennings [30] at 163°C for the highest of the PLLA molecular weights investigated, that is, for a polymer with viscometric molecular weight $M_v = 150$ kDa, while lower molecular weight polymers presented only a regime II crystallization type.

Tsuji and Ikada [35] studied the effect of different thermal treatments and annealing histories on solution cast PLLA films, which resulted in materials with different morphologies and physical properties. In particular, annealing was performed on films as (A) cast; (B) cast and molten; and (C) cast, molten, and quenched. Differences in crystallization were mainly attributed to the presence of preexisting spherulite nuclei before annealing, with the B film having higher developed total crystallinity content at any annealing temperature, resulting in higher mechanical strength. An increase in crystallinity was observed in the annealing temperature range 100–160°C.

In a later work, Mazzullo et al. [34] have also found a regime III governed crystallization starting at 140°C, with K_{gIII}/K_{gII} equal to 3.13. Several authors have then confirmed the presence of three distinct crystallization regimes, starting at different temperatures and with different constants [36, 41–43].

The crystallization mode of PLLA has also been analyzed by using the Avrami equation [71, 72]

$$X_c = 1 - \exp(-kt^n) \tag{9.7}$$

By measuring the fraction of crystallized material, X_c, with time t, a value of the constant n equal to 4 was evaluated by Miyata and Masuko [37] who observed, in nonisothermal crystallization experiments from the melt, a remarkable increase in the polymer crystallization at decreasing cooling rates and a maximum value of the isothermal crystallization rate at 105°C. A similar trend was observed by Iannace and Nicolais [36]. However, these results could be affected by the polymer thermal degradation induced at a low cooling rates, as previously described by Migliaresi et al. [27].

9.4 FIBERS

First studies about the fabrication of PLA fibers were made by Kulkarni et al. [13, 14] and Kalb and Pennings [23]. PLA fibers can be produced by melt and solution spinning [24, 73–75]. The two methods generate fibers with different mechanical properties and degradation rate, which can be explained in terms of the different developed crystal morphologies [47, 73, 76]. In both cases, the high shear rate induced orientation and chain alignment that in turn induced crystallization. Wide-angle X-ray scattering revealed the presence of two distinct crystal modifications in solution-spun fibers and in particular the origin of a so-called β-structure in hot drawn fibers. The β-structure seems to correspond to fibrillar morphology and bears most of the load applied to the fibers. Recently, it has been found that the redrawing of highly oriented PLLA film induces the transformation of the α-form crystallites into the β-form [77]. PLLA solution-spun fibers have better mechanical properties and also higher hydrolytic degradation stability [75].

Crystallinity developed in melt- and solution-spun fibers is reported in Figure 9.11 as a function of the applied draw ratio. In both cases, for draw ratios higher than 8–10, a maximum value of crystallinity equal to about 65% and 44% was reached for melt- and solution-spun fibers, respectively [76, 78].

Similar results were also found in the case of films where, after drawing, crystallinity significantly increased up to about 55% [79].

Melt spinning imparts intense thermal and mechanical stress on PLLA, resulting in a large reduction in molar mass that can reach 30–70% [24, 76]. Hence, when considering the crystallizability of polymer fibers, the effects of molecular weight and the thermal and mechanical drawing should be considered.

The relatively low molecular weight of melt-spun fiber, between 30 and 150 kDa, results in high crystallizability especially during drawing. In a double-step process of fiber spinning followed by fiber drawing, crystallization from

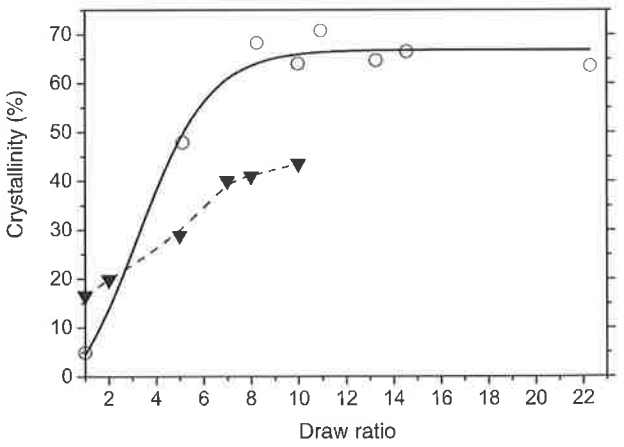


FIGURE 9.11 Crystallinity of melt-spun PLLA fiber drawn at 160°C (○) and crystallinity of solution-spun PLLA fiber drawn at 190°C (▼) as a function of draw ratio.

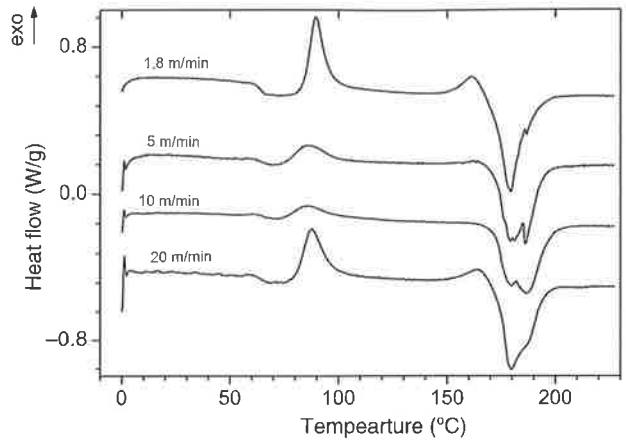


FIGURE 9.12 DSC curves of melt-spun PLLA fibers collected at different rates, as indicated. Reprinted from Ref. 76. Copyright 1997, with permission from Elsevier.

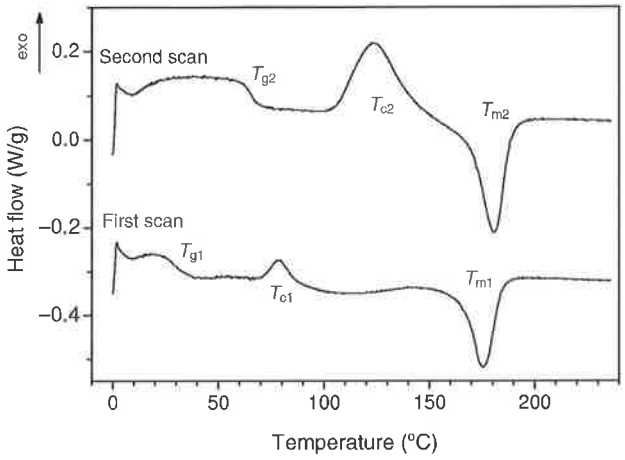


FIGURE 9.13 First and second DSC scans of as-spun PLLA fibers produced by solution spinning (5% chloroform solution).

the melt should be properly controlled in order to preserve the ability for further orientation and crystallization. It was reported that depending on the fiber collecting rate, the crystallinity of as-spun fiber initially increased up to about 35%, and then decreased as the fiber collecting rate increased, due to the faster cooling rate of the higher surface area of the lower diameter fibers. Figure 9.12 shows the thermograms of PLLA melt-spun fibers collected at 1.8, 5, 10, and 20 m/min.

The different amorphous phase content is initially evidenced by the various ΔC_p at the T_g, 0.36, 0.19, 0.14, and 0.30 J/(g K). Moreover, it should be noted that the crystallization peak of these melt-spun fibers occurred during heating in the range of about 80–120°C, significantly lower than that of completely amorphous PLLA reported in Figure 9.1, with direct dependence on the preexistent nucleating crystalline domains and the oriented polymer structure. At higher temperatures, a small exothermal peak of secondary crystallization at about 160°C precedes the melting. As shown in Figure 9.12, curves revealed two melting peaks, the higher temperature one just indicated by a shoulder in the highest rate collected fibers. The melting at about 188°C was due to crystallinity developed during the melt spinning process, whereas the peak at 180°C corresponded to the melting of crystals generated during the DSC analysis. The percentage crystallinity of the fiber can be evaluated as 5%, 30%, 37%, and 10% for spinning process of 1.8, 5, 10, and 20 m/min, respectively.

The drawing temperature is selected above the T_g in order to modify the amorphous phase in the rubbery state; the initial crystallinity, the nucleation and growth rate according to the crystallization regimes I–III, the polymer chain mobility, and the polymer molecular weight are important factors for optimization of fiber orientation and crystallization. Typically, PLLA melt-spun fibers after drawing at 160°C reach a crystallinity of about 50–70% [24, 80].

In the case of solution spinning, the crystallinity of undrawn as-spun fiber was typically 30–40%, higher than that of melt-spun fibers (compare data of Figures 9.12 and 9.13), due to the lower spinning and cooling rate, and in general as a consequence of the more favorable conditions of solvent crystallization. Solvent, in fact, acts as a plasticizer, resulting in a higher chain rearrangement capability.

At the same time, the relatively high molecular weight (between 300 and 900 kDa) inhibits the development of high crystallinity due to the lower polymer chain mobility [78,81, 82]. Figure 9.14 shows the first and second DSC scans of as-spun PLLA fibers produced from dry spinning. Low T_g due to the residual solvent that acts as a plasticizer, and low T_c and T_m were observed in the first scan. In the second DSC scan after a mass loss of about 15% attributable to solvent remotion, a T_g of 65°C and crystallization and melting peaks at 140 and 180°C, respectively, with a crystallinity of about 25%, were observed.

These solution as-spun fibers can be drawn at a higher drawing temperature, above the expected T_m (this is possible due to the high polymer molar mass and initial crystallinity). The results of DSC analysis revealed, after drawing at temperatures between 160 and 210°C, the formation of a double crystalline structure, with two melting peaks at about 160–170 and 190–200°C, as summarized in Table 9.3 and shown in selected thermograms of Figure 9.14.

The higher the drawing temperature, the higher the total crystallinity and the enthalpy of the first melting peak at about 160–170°C, thus suggesting the formation of the β--phase, as previously indicated by Pennings and coworkers, in coexistence with the α-phase [47, 73, 74, 82].

At the same time, the T_g was found to increase with the drawing temperature, reaching about 100°C, as a consequence of the high orientation of the crystallized fibers. Moreover, the progressive and remarkable reduction of ΔC_p from 0.1 to about 0.05 J/(g K) indicates both high packing

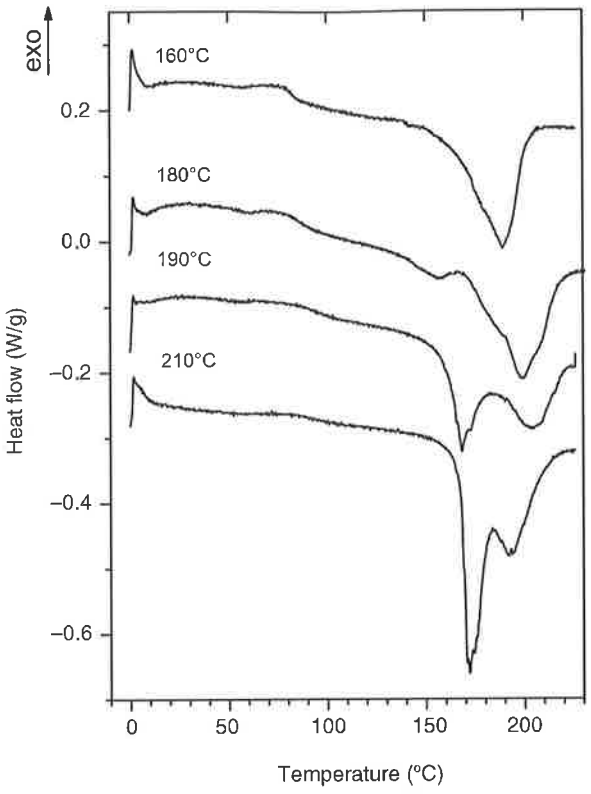


FIGURE 9.14 DSC thermograms of solution-spun fibers after drawing at various temperatures (glass transition temperature and various melting peaks are evident) [78].

and low mobility of the amorphous phase above T_g, once again as a consequence of the high orientation of the high molecular weight drawn PLLA fibers.

Copolymerization of L-lactide with other analogous cyclic lactones, such as DL-lactide, D-lactide, glycolide, or ε-caprolactone, produces polymers with relatively random distribution of comonomers. The T_g of PLA copolymers decreases proportionally to the content of the glycolide or ε-caprolactone comonomer to some extent. Moreover, the presence of stereochemical defects in PLLA reduces T_m, rate of crystallization, and extent of crystallization of the resulting polymer. Reed and Gilding reported in 1979 a sharp reduction of melting point to 120°C with the addition of 20% glycolide, with no crystallization occurring if glycolide content reached 25% [22]. Figure 9.15a and b summarizes some of their results.

Analogously, the L/DL-lactide copolymers present an almost linear T_m depression, from 178°C for pure PLLA to 115°C for the 70/30 copolymer, and a T_g decrease from 63 to about 55°C, as shown in Figure 9.16.

9.5 HYDROLYTIC DEGRADATION

The degradation kinetics of PLLA is largely affected by its crystallinity. As is known, degradation of PLA proceeds via hydrolysis, which is in turn controlled by the water diffusion in the free volume amorphous phase. In addition to crystallinity, other factors such as molecular weight, surface/volume ratio, purity, and chain orientation can greatly affect degradation kinetics [7].

Migliaresi et al. [83] compared the hydrolytic degradation of different molecular weight and crystallinity PLLAs, obtained by quenching or annealing treatments.

As reported in Figure 9.17 for two different molecular weight PLLA polymers, as degradation proceeds, crystallinity increases reaching an almost equal value for the two polymers despite their largely different initial crystallinities, that is, $X = 46\%$ for PLLA (153 kDa) and $X = 6\%$ for PLLA (103 kDa). This behavior was not attributable to the loss of amorphous degraded materials, because no appreciable mass loss was detected during the experiment.

A concomitant phenomenon associated with the molar mass reduction was the plasticizing effect of the water molecules diffusing into the amorphous regions, which provoked an increase of the chain segmental motion. Ultimately, the crystallinity increased when chain length became short enough to enable spatial rearrangement of the original amorphous regions in crystalline domains.

This degradation-induced crystallization is a very important drawback for the biomedical use of PLLA as an implant

TABLE 9.3 Glass Transition Temperature (T_g) and Change of Specific Heat at T_g (ΔC_p), Melting Peak Temperature (T_m) and Enthalpy (ΔH_m), and Crystallinity of Solution-Spun Fibers After Drawing at Various Temperatures

Drawing Temperature (°C)	T_g (°C)	ΔC_p (J/(g K))	First Melting Peak		Second Melting Peak		Crystallinity (%)
			T_m (°C)	ΔH_m (J/g)	T_m (°C)	ΔH_m (J/g)	
160	83	0.13	–	–	190	29	31
170	81	0.12	–	–	189	29	32
180	87	0.11	155	5	199	27	34
190	98	0.09	169	16	203	17	35
200	92	0.09	167	17	201	21	41
210	97	0.04	172	26	195	18	47

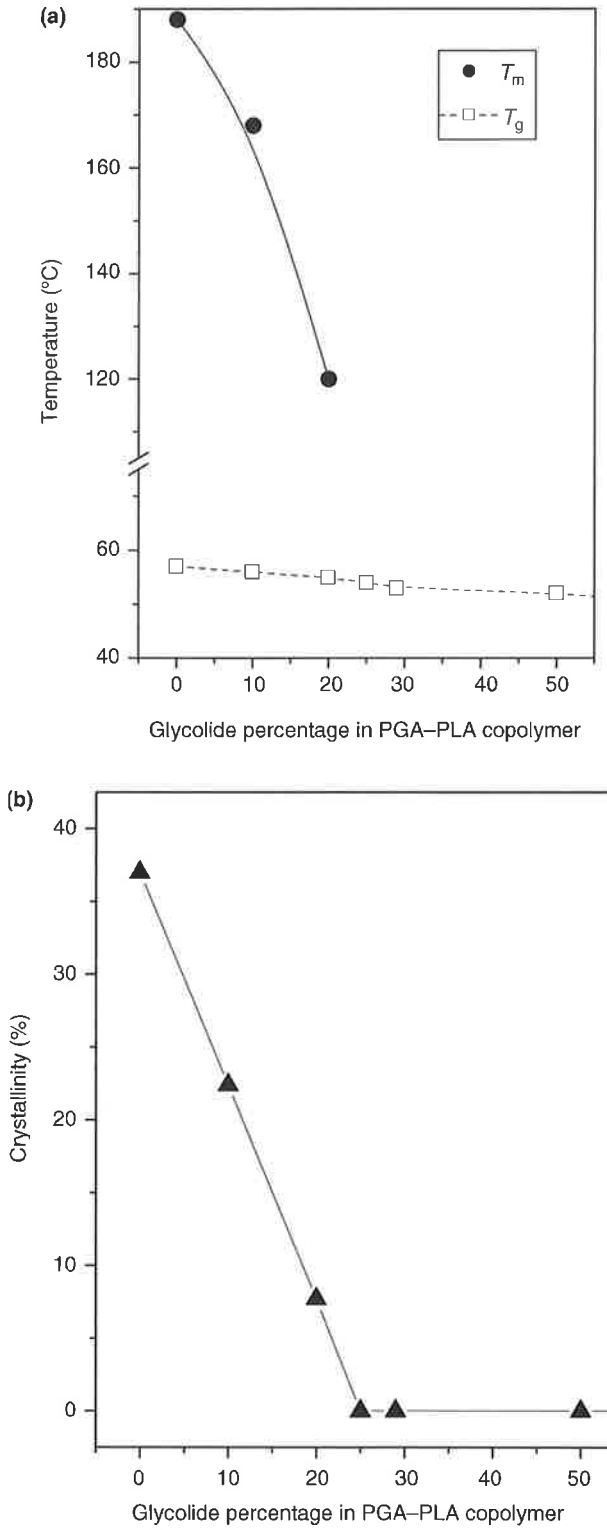


FIGURE 9.15 Effect of composition on T_g, melting temperature (a) , and crystallinity (b) of L-lactide-*co*-glycolide copolymers as a function of glycolide content (adapted from literature). Reprinted from Ref. 22. Copyright 1979, with permission from Elsevier.

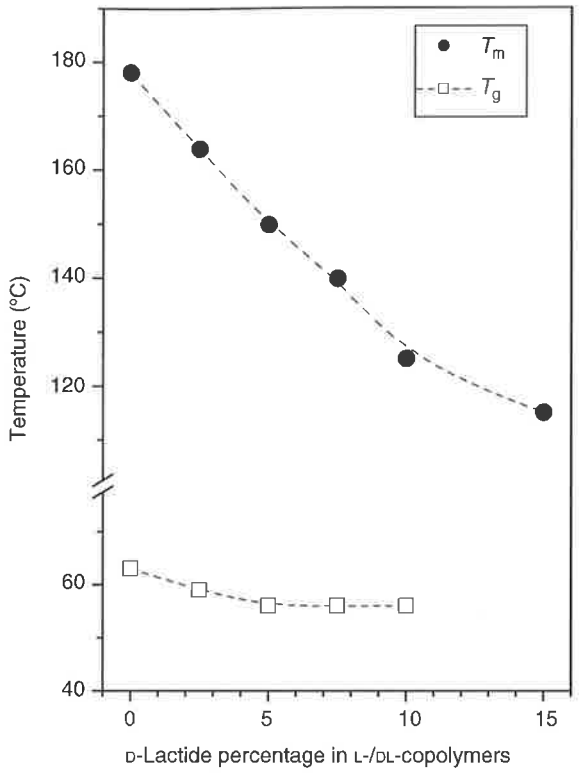


FIGURE 9.16 T_g and T_m of poly-L-D, L-lactide as a function of D, L-lactide content (adapted from Ref. 31 and authors data).

material, which can last in the implant site for a very long time [84, 85]. Pistner et al. [84] observed *in vivo* an increase of crystallinity that reached 96% after 52 weeks of implantation in the dorsal muscle of rats. Even though they attributed such increase to the preferential degradation and cleavage of the amorphous regions, it is plausible that also in this case degradation induced a rearrangement of part of the amorphous regions into a crystalline structure, as

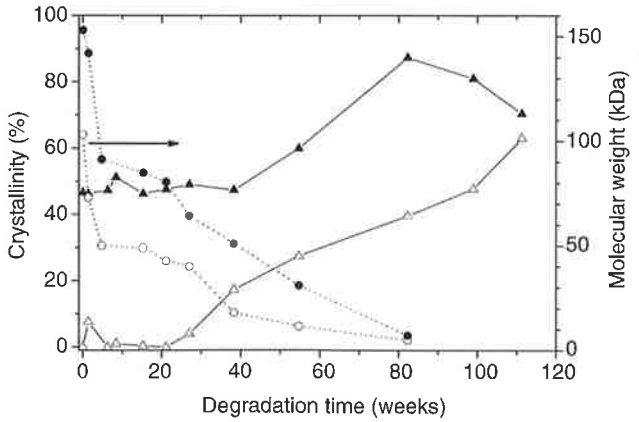


FIGURE 9.17 Crystallinity percentage (△, ▲) and molecular weight (○, ●) as a function of degradation time in Ringer solution at 37°C for PLLA samples of initial low (open symbols) and high (filled symbols) crystallinity, respectively (adapted from Ref. 83).

previously described by Migliaresi et al. [27]. The excessive longevity of PLLA *in vivo*, which is considered the major drawback of the polymer for biomedical applications, can be in part related to the observed *in vivo* degradation-induced crystallization that slows down the hydrolytic attack on the compact stable crystalline regions. Also, residues of PLLA *in vivo* have been observed after 7 years of implantation. Also worth noting for biomedical uses of PLLA is the increase in crystallinity due to gamma ray irradiation with the formation of new thin crystal lamellae [86].

REFERENCES

1. T. H. Barrows, *Clin. Mater.* **1986**, *1*, 233–257.
2. I. Engelberg, J. Kohn, *Biomaterials* **1991**, *12*, 292–304.
3. M. Vert, G. Schwarch, J. Coudane, *J. Macromol. Sci. Pure Appl. Chem.* **1995**, *A32*, 787–792.
4. W. Amass, A. Amass, B. Tighe, *Polym. Int.* **1998**, *47*, 89–144.
5. Y. Ikada, H. Tsuji, *Macromol. Rapid Commun.* **2000**, *21*, 117–132.
6. D. A. Garlotta, *J. Polym. Environ.* **2001**, *9*, 63–84.
7. L. Fambri, C. Migliaresi., K. Kesenci, E. Piskin, Biodegradable polymers, in: R. Barbucci (Ed.), *Integrated Biomaterials Science*, Kluwer Plenum Publications, New York, 2002, Chapter 4, pp. 119–187.
8. H. Tsusj, Polylactide, in: Y. Doi, A. Steinbuchel (Eds.), *Biopolymers. Polyesters III. Applications and Commercial Products*, Wiley-VCH Verlag GmbH, Weinheim, 2002, Chapter 5, pp. 129–177.
9. N. Kumar, A. Ezra, T. Ehrenfroind, M. Y. Krasko, A. J. Domb, Biodegradable polymers, medical applications, in: H. F. Mark (Ed.), *Encyclopedia of Polymer Science & Technology*, 3rd edition, Wiley, Hoboken, NJ, 2003, Chapter 5, pp. 263–285.
10. R. von Oepen, W. Michaeli, *Clin. Mater.* **1992**, *10*, 21–28.
11. B. Gupta, N. Revagade, J. Hilborn, *Prog. Polym. Sci.* **2007**, *32*, 455–482.
12. L. T. Lim, R. Auras, M. Rubino, *Prog. Polym. Sci.* **2008**, *33*, 820–852.
13. R. K. Kulkarni, K. C. Pani, C. Neuman, F. Leonard, *Arch. Surg.* **1966**, *93*, 839–843.
14. R. K. Kulkarni, E. G. Moore, A. F. Hegyeli, F. Leonard, *J. Biomed. Mater. Res.* **1971**, *5*, 169–171.
15. A. P. Gupta, V. Kumar, *Eur. Polym. J.* **2007**, *43*, 4053–4074.
16. A. L. Lehninger, *Biochemistry*, 3rd edition, Worth Publishers Inc., New York, 1977.
17. J. Lunt, *Polym. Degrad. Stabil.* **1998**, *59*, 145–152.
18. T. Maharana, B. Mohanty, Y. S. Negi, *Prog. Polym. Sci.* **2009**, *34*, 99–124.
19. C. W. Lee, *Fibers Polym.* **2007**, *8*, 571–578.
20. T. M. Ovitt, G. W. Coates, *J. Am. Chem. Soc.* **1999**, *121*, 4072–4073.
21. E. W. Fisher, H. J. Sterzel, G. Wegner, *Kolloid Z. Z. Polym.* **1973**, *251*, 980–990.
22. D. K. Gilding, A. M. Reed, *Polymer* **1979**, *20*, 1459–1464.
23. B. Kalb, A. J. Pennings, *Polymer* **1980**, *21*, 607–612.
24. S. H. Hyon, K. Jamshidi, Y. Ikada, Melt spinning of poly-L-lactide and hydrolysis of the fibre *in vitro*, in: S. W. Shalaby, A. S. Hoffmann, B. D. Ratner, T. A. Horbett (Eds.), *Polymers as Biomaterials*, Plenum Press, New York, 1984, pp. 51–65.
25. Y. Ikada, K. Jamshidi, H. Tsuji, S. H. Hyon, *Macromolecules* **1987**, *20*, 904–906.
26. H. Younes, D. Cohn, *Eur. Polym. J.* **1988**, *24*, 765–773.
27. C. Migliaresi, A. De Lollis, L. Fambri, D. Cohn, *Clin. Mater.* **1991**, *8*, 111–118.
28. A. Celli, M. Scandola, *Polymer* **1992**, *33*, 2699–2703.
29. G. L. Loomis, J. R. Murdoch, K. H. Gardner, *Polym. Prepr.* **1990**, *31*(2), 55.
30. R. Vasanthakumari, A. J. Pennings, *Polymer* **1983**, *24*, 175–178.
31. K. Jamshidi, S. H. Hyon, Y. Ikada, *Polymer* **1988**, *29*, 2229–2234.
32. C. Migliaresi, D. Cohn, A. De Lollis, L. Fambri, *J. Appl. Polym. Sci.* **1991**, *43*, 83–95.
33. C. Marega, A. Marigo, V. Di Noto, R. Zannetti, A. Martorana, G. Paganetto, *Makromol. Chem.* **1992**, *193*, 1599–1606.
34. S. Mazzullo, G. Paganetto, A. Celli, *Prog. Colloid Polym. Sci.* **1992**, *87*, 32–34.
35. H. Tsuji, Y. Ikada, *Polymer* **1995**, *36*, 2709–2716.
36. S. Iannace, L. Nicolais, *J. Appl. Polym. Sci.* **1997**, *64*, 911–919.
37. T. Miyata, T. Masuko, *Polymer* **1998**, *39*, 5515–5521.
38. J. J. Kolstad, *J. Appl. Polym. Sci.* **1996**, *62*, 1079–1091.
39. G. Perego, G. D. Cella, C. Bastioli, *J. Appl. Polym. Sci.* **1996**, *59*, 37–43.
40. J. R. Sarasua, R. E. Prud'homme, M. Wisniewski, A. Le Borgne, N. Spassky, *Macromolecules* **1998**, *31*, 3895–3905.
41. M. L. Di Lorenzo, *Polymer* **2001**, *42*, 9441–9446.
42. M. L. Di Lorenzo, *Eur. Polym. J.* **2005**, *41*, 569–575.
43. M. L. Di Lorenzo, *J. Appl. Polym. Sci.* **2006**, *100*, 3145–3151.
44. Y. Wang, J. F. Mano, *Eur. Polym. J.* **2005**, *41*, 2335–2342.
45. Y. Yuryev, P. Wood-Adams, M. C. Heuzey, C. Dubois, J. Brisson, *Polymer* **2008**, *49*, 2306–2320.
46. P. De Sanctis, A. Kovacs, *Biopolymers* **1968**, *6*, 299–306.
47. W. Hoogsteen, A. R. Postema, A. J. Pennings, G. ten Brinke, P. Zugenmaier, *Macromolecules* **1990**, *23*, 634–642.
48. L. Cartier, T. Okihara, Y. Ikada, H. Tsuji, J. Puiggali, B. Lotz, *Polymer* **2000**, *41*, 8909–8919.
49. J. R. Dorgan, J. Jansen, M. P. Clayton, *J. Rheol.* **2005**, *49*, 607–619.
50. A. J. Ninjenhuis, D. W. Grijpma, A. J. Pennings, *Polym. Bull.* **1991**, *26*, 71–77.
51. L. E. Nielsen, R. F. Landel, *Mechanical Properties of Polymers and Composites*, 2nd edition, Marcel Dekker, New York, 1994.
52. M. P. Seppe, *Rapra Rev. Rep.* **1997**, *8*, 22.
53. S. Diez-Gutierrez, M. A. Rodriguez-Perez, J. A. Saja, J. I. Velasco, *Polymer* **1999**, *40*, 5345–5353.

54. L. Fambri, K. Kesenci, C. Migliaresi, *Polym. Compos.* **2003**, *24* (1), 100–108.
55. D. W. van Krevelen, *Properties of Polymers*, 3rd edition, Elsevier, Amsterdam, 1998, p. 402.
56. L. C. E. Struik, *Physical Aging of Amorphous Polymers and Other Materials*, Elsevier, Amsterdam, 1978.
57. T. Ke, X. Sun, *J. Appl. Polym. Sci.* **2003**, *89*, 1203–1210.
58. J. Y. Nam, S. S. Ray, M. Okamoto, *Macromolecules* **2003**, *36*, 7126–7131.
59. D. M. Bigg, *Conference Proceedings ANTEC: Annual Technical Conference*, Society of Plastics Engineers, Nashville, TN, 2003, pp. 2816–2822.
60. J. Y. Nam, M. Okamoto, H. Okamoto, M. Nakano, A. Usuki, M. Matsuda, *Polymer* **2006**, *47*, 1340–1347.
61. N. Kawamoto, A. Sakai, T. Horikoshi, T. Urushihara, E. Tobita, *J. Appl. Polym. Sci.* **2007**, *10*, 198–203.
62. H. Li, M. A. Huneault, *Polymer* **2007**, *48*, 6855–6866.
63. S. Jacobsen, H. G. Fritz, *Polym. Eng. Sci.* **1999**, *39*, 1303–1310.
64. O. Martin, L. Averous, *Polymer* **2001**, *42*, 6209–6219.
65. N. Ljungberg, B. Wesselen, *J. Appl. Polym. Sci.* **2002**, *86*, 1227–1234.
66. Z. Kulinski, E. Piorkowska, *Polymer* **2005**, *46*, 10290–10300.
67. Z. Ren, L. Dong, Y. Yang, *J. Appl. Polym. Sci.* **2006**, *101*, 1583–1590.
68. I. Pillin, N. Montrelay, Y. Grohens, *Polymer* **2006**, *47*, 4676–4682.
69. J. I. Lauritzen, J. D. Hoffman, *J. Appl. Phys.* **1973**, *44*, 4340–4352.
70. J. D. Hoffman, G. T. Davis, J. I. Lauritzen, in: N. B. Hannay (Ed.), *Treatise on Solid State Chemistry*, Vol. 3, Plenum Press, New York, **1976**, Chapter 7.
71. M. J. Avrami, *J. Chem. Phys.* **1940**, *8*, 212–224.
72. M. J. Avrami, *J. Chem. Phys.* **1941**, *9*, 177–184.
73. B. Eling, S. Gogolewski, A. J. Pennings, *Polymer* **1982**, *23*, 1587–1593.
74. S. Gogolewski, A. J. Pennings, *J. Appl. Polym. Sci.* **1983**, *28*, 1045–1061.
75. C. Migliaresi, L. Fambri, *Macromol. Symp.* **1997**, *123*, 155–161.
76. L. Fambri, A. Pegoretti, R. Fenner, S. D. Incardona, C. Migliaresi, *Polymer* **1997**, *38*, 79–85.
77. K. Takahashi, D. Sawai, T. Yokoyama, T. Kanamoto, S.-H. Hyon, *Polymer* **2004**, *45*, 4969–4976.
78. L. Fambri, A. Pegoretti, M. Mazzurana, C. Migliaresi, *J. Mater. Sci. Mater. Med.* **1995**, *5*, 679–684.
79. A. Fujimori, N. Ninomiya, T. Masuko, *Polym. Adv. Technol.* **2008**, *19*, 1735–1744.
80. A. Pegoretti, L. Fambri, C. Migliaresi, *J. Appl. Polym. Sci.* **1997**, *64*, 213–223.
81. I. Horacek, V. Kalisek, *J. Appl. Polym. Sci.* **1994**, *54*, 1751–1757.
82. J. W. Leenslag, A. J. Pennings, *Polymer* **1987**, *28*, 1695–1702.
83. C. Migliaresi, D. Cohn, L. Fambri, *J. Biomater. Sci. Polym. Ed.* **1994**, *5*(6), 591–606.
84. H. Pistner, D. R. Bendix, J. Muhling, J. F. Reuther, *Biomaterials* **1993**, *14*, 291–298.
85. J. E. Bergsma, W. C. de Bruijn, F. R. Rozema, R. R. M. Bos, G. Boering, *Biomaterials* **1995**, *16*, 25–31.
86. D. Mililevic, S. Trifunovic, S. Galovic, E. Suljiovrujic, *Radiat. Phys. Chem.* **2007**, *76*, 1376–1380.